

# Fully Additive Fabrication of Electrically Anisotropic Multilayer Materials Based on Sequential Electrodeposition

Michael Synodis<sup>1</sup>, Jun Beom Pyo, *Graduate Student Member, IEEE*, Minsoo Kim<sup>2</sup>, *Member, IEEE*, Hanju Oh, *Member, IEEE*, Xuan Wang, and Mark. G. Allen<sup>3</sup>, *Fellow, IEEE*

**Abstract**—MEMS-enabled multilayer composites, in which microfabrication is used to create micron-scale thickness layers within the volume of meso-scale thickness structures, can be exploited to create materials with highly anisotropic electromagnetic properties. Such materials have utility in both sensing and energy applications, including electrostatic and magnetic energy storage and conversion. A fabrication challenge in realizing these classes of materials lies in the size-scale disparity between the thickness of an individual layer and the desired thickness of the final anisotropic material. We demonstrate a fully additive sequential electrochemical deposition approach for such structures, which enables scalable composite volume while maintaining micron-scale individual layer thicknesses. Alternating metal and polymer layers, which exhibit very different electrical conductivities, are continuously electrodeposited in batch-scale. Individual layer thicknesses are controlled by deposition currents and times, while lateral extents are defined by lithographically defined molds. The fabrication process is illustrated using electrodeposited NiFe alloys and polypyrrole, and the anisotropy of electrical conductivity is assessed for potential use of these structures as magnetic cores for high frequency switching converters. Due to the relatively resistive polypyrrole layers, electrical anisotropy of lateral to vertical conductivity exceeding  $10^6$  was achieved. This approach offers a solution-based, microfabrication compatible, and manufacturable route to functional composite materials that exhibit high electrical anisotropies. [2020-0256]

**Index Terms**—MEMS, anisotropic structures, conductive polymer, electrodeposition, multilayer composites.

Manuscript received June 30, 2020; revised September 2, 2020; accepted September 8, 2020. Date of publication September 22, 2020; date of current version December 1, 2020. This work was supported in part by the Singh Center for Nanotechnology, through the NSF National Nanotechnology Coordinated Infrastructure Program, under Grant NNCI-1542153, and in part by the Enachip, Inc. Subject Editor G. Stemme. (*Corresponding author: Michael Synodis.*)

Michael Synodis was with the Department of Chemical and Biomolecular Engineering, University of Pennsylvania, Philadelphia, PA 19104 USA. He is now with Exponent, Inc., Menlo Park, CA 94025 USA (e-mail: msynodis@seas.upenn.edu).

Jun Beom Pyo, Xuan Wang, and Mark. G. Allen are with the Department of Electrical and Systems Engineering, University of Pennsylvania, Philadelphia, PA 19104 USA (e-mail: junpyo@seas.upenn.edu; wxuan@seas.upenn.edu; mallen@seas.upenn.edu).

Minsoo Kim and Hanju Oh were with the Department of Electrical and Systems Engineering, University of Pennsylvania, Philadelphia, PA 19104 USA. They are now with Apple, Inc., Cupertino, CA 95014 USA (e-mail: novamagic@gmail.com; hanjuoh5@gmail.com).

Color versions of one or more of the figures in this article are available online at <https://ieeexplore.ieee.org>.

Digital Object Identifier 10.1109/JMEMS.2020.3023347

## I. INTRODUCTION

LAMINATED multilayer structures comprising alternating layers of metallic laminations and insulating interlamination materials can be found in many applications such as capacitors [1], induction coils [2], laminated magnetic cores [3], [4], and vertically integrated electrodes for sensors [5]. Structures comprised of these sequentially alternating layers can display highly anisotropic material characteristics [6]. In particular, MEMS-scale laminated cores that consist of micron-thick, electrically insulated, soft magnetic metallic alloys are regarded as a potential enabler of on-chip miniaturized magnetic devices (i.e., inductors and transformers) that will operate at high frequencies, handling watt-level power within small device volumes. The electrical anisotropy of the laminated cores, in particular the low electrical conductivity in the direction orthogonal to the flow of magnetic flux, enables operation of these electrically conducting materials even at high frequency. Achieving isolated magnetic layers in a core, in which the magnetic layer thicknesses are less than the skin depth of the magnetic material at the frequency of operation is critical, both to ensure conduction of magnetic flux through the cross section of the layers as well as to suppress generation of eddy currents within the volume of each layer. Also critical to reducing these losses is sufficient prevention of eddy current propagation from magnetic layer to magnetic layer through the intralayer isolation. Thus, independently engineering the electrical conductivity anisotropy in the vertical and lateral directions is key to optimizing core performance.

At the high frequencies typical of advanced switching power converters (e.g., MHz and above), the skin depths of typical conducting magnetic alloys are on the order of microns. Thus, MEMS-based fabrication approaches are desirable. MEMS-scale laminated structures are typically fabricated by deposition-based methods, since traditional lamination approaches based on milling, cutting, and stacking processes exhibit technical difficulties in achieving layers with desired microscale thicknesses. Sequential, “top-down” physical vapor deposition of magnetic and insulating material can create laminated structures with controlled, nanoscale individual layer thicknesses [7]; however, its relatively poor scalability (due to high built-in stress) and high cost (due to non-selective, vacuum-based deposition processes) may

limit the total thicknesses achievable in the lamination stack.

As an alternative, electrodeposition-based MEMS lamination processes have been developed. Direct electrodeposition of metallic and electrically insulating materials (which would be analogous to the sequential physical vapor deposition), especially selective deposition in lithographic molds, is challenging, since the deposition of an insulating layer tends to inhibit subsequent sequential electrodeposition. Although in principle electroless deposition could be used to form subsequent metallic layers on an insulating lamination layer, the multi-step electroless deposition process and need to remove/prevent material growth outside the mold adds complexity. Further, the materials set becomes limited to those compatible with electroless deposition. Hence, typical electrodeposition-based lamination technologies are completed by subtractive processes in which an electrodeposited multilayer structure, comprised of alternating conducting structural and sacrificial interlamination layers, is utilized [3], [8]. After completion of the multilayer electrodeposition, the sacrificial layers are selectively removed from the structure, leaving the suspended structural layers supported, e.g., by lithographically defined anchors. An additive process in which direct electrodeposition of the active and insulating materials in a laminated structure is performed would remove the need for this subtractive lateral etch process, enabling batch scale processing of material composites with anisotropic properties. Processes have been developed in which electrically insulating interlayers are patterned and then subsequently coated with active metals, but a direct additive deposition process has not yet been effectively demonstrated [9], [10].

In order to design a laminated structure with electrically anisotropic properties, the range of tolerable conductivities of interlamination insulation materials is analyzed. For a capacitor application, insulators with very high resistivities are required. On the contrary, materials of intermediate conductivity may be utilized as an insulation layer in laminated magnetic cores, even at MHz frequencies, and still suppress eddy currents. For example, under certain conditions if the ratio of conductivities of the magnetic and insulation layers in the core is on the order of  $10^6$ , efficient operation as MEMS-scale magnetic cores in the MHz range is possible (see [11] for a full treatment). This, in principle, sets the *maximum* tolerable conductivity for the insulation material. To determine the *minimum* tolerable conductivity for the insulation material, fabrication constraints should be examined.

Consider the electrodeposition of a multilayer stack of alternating metallic and (relatively) insulating materials within a photoresist mold of area  $A$ , with an electrodeposition current density  $J$  required to grow the layers at reasonable rates (and appropriate compositions, as applicable). As the current flows through the stack to form subsequent layers, there will be a voltage drop across the stack. If the maximum tolerable voltage drop is denoted by  $V_{drop, max}$ , and it is assumed that all of the voltage drop occurs across the relatively highly resistive interlamination layers, the minimum conductivity to achieve multilayer electrodeposition can be expressed as

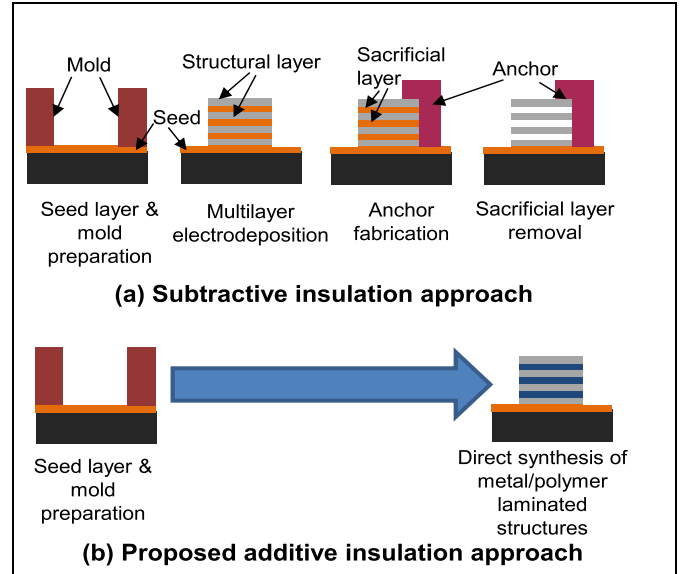


Fig. 1. Schematics of multilayer composite fabrication processes based on (a) subtractive interlayer insulation and (b) additive, polymeric insulation.

shown in Equation 1:

$$\sigma_{min} = \frac{jnt_{ins}}{V_{drop,max}} \quad (1)$$

where  $n$  is the number of laminations, and  $t_{ins}$  is the thickness of each (nominally identical thickness) insulating layer.

For typical magnetic alloys electrodeposited at a potential of 2 – 3V and typical current densities of 10 mA/cm<sup>2</sup>, a maximum voltage drop of 0.05V is considered a small perturbation [12]. Substitution into (1), and assuming a typical lamination stack of 10 layer sets, suggests a minimum conductivity of  $10^{-2}$ – $10^{-1}$  S/m for micron scale insulation layer thicknesses. Since typical metallic material conductivities are on the order of  $10^6$ – $10^7$  S/m the aforementioned requirement (for magnetic applications) of a  $10^6$  ratio of metal to insulator electrical conductivity (for relatively similar thicknesses of lamination and interlayer) suggests a maximum interlayer conductivity of 10 S/m. Thus, an interlayer material of intermediate conductivity ( $\sim 1$  S/m) may satisfy not only the sufficiency of further electrodeposition criterion, but also the magnetic criterion. Of course, other applications may have less stringent requirements on maximum electrical conductivity of the interlayer; also, voltage sources could be continually adjusted as more layers are deposited to maintain electrodeposition currents in the face of increasing interlayer resistance. However, this guideline presents a useful order-of-magnitude target for the required electrical anisotropy of these materials.

## II. FABRICATION APPROACH

Figure 1 shows a schematic of previous fabrication approaches to create metal/polymer laminated structures, and contrasts these approaches with the proposed fully additive approach. In previous work (Figure 1a), sequential electrodeposition of structural metallic layers and highly conducting

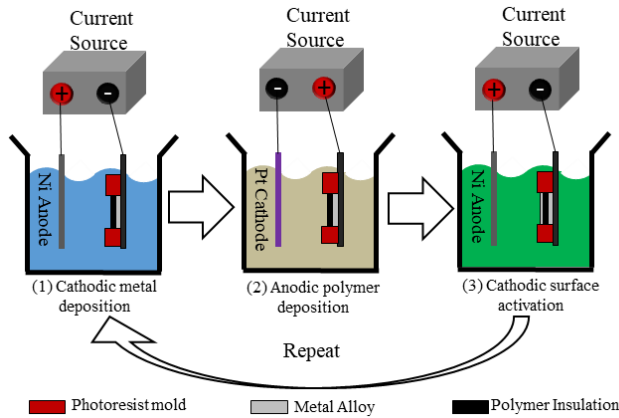


Fig. 2. Schematic of the proposed additive fabrication method, which consists of repeating steps of metallic functional material deposition, conductive polymer electropolymerization, and polymer surface activation.

sacrificial layers (typically also metallic) results in a multilayer stack. Selective subtractive removal of the sacrificial layer, followed by optional impregnation of the spaces between metallic structural layers, results in a metal/polymer (or metal/air) multilayer composite. In contrast, the fully additive approach (Figure 1b) simply fills the electroplating mold with alternating layers of highly conductive metals and electrodepositable polymers of intermediate conductivity.

Referring to Figure 1b, fabrication begins with seed layer and mold preparation. A layer of lift off resist (LOR-3A, MicroChem) is spin cast on a glass or silicon substrate, and a seed layer of 50nm Ti, 600nm Cu, and 50nm Ti is sputtered onto the resist. Typical substrate sizes used for this work were 4-inch silicon or 2×3 inch glass wafers. The adhesion between the bottom titanium layer and the LOR-3A is sufficiently strong to perform multilayer deposition, while it is sufficiently weak to mechanically detach the fabricated multilayer materials from the substrate, post deposition, for subsequent electrical characterization of the deposited materials. After seed layer preparation, an electrically insulating photoresist mold (AZ4620, MicroChem) is lithographically patterned on the seed layer to define the lateral extents of the multilayer cores (Figure 1b, left).

Following mold development, the uppermost Ti of the seed layer is removed, and alternating electrodeposition of metal and interlayer material within the mold is performed (Figure 2). A deposition cycle comprises (1) the electrodeposition of metallic functional material, (2) electropolymerization of the polymer interlayer, and (3) polymer surface activation (i.e., electrodeposition of a thin metallic layer at a low deposition potential) for subsequent magnetic material deposition. Since all deposition reactions are highly selective to conductive surfaces, the deposition only occurs within the mold (if the mold thicknesses are larger than the total multilayer core thickness). The current densities in the respective electrolytes are fixed during deposition while the individual layer thicknesses of metal and polymer are controlled by deposition time. The metal/polymer deposition cycle is repeated as desired; typically, the deposition process begins and ends with magnetic material deposition. Hence, the number of metallic

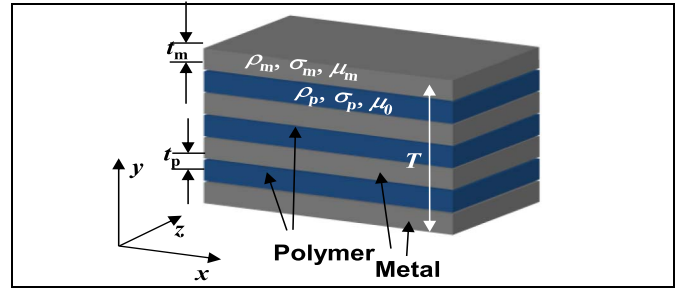


Fig. 3. Schematic of a laminated structure. Individual layer thickness of metal and polymer are  $t_m$  and  $t_p$ . The resistivity, conductivity, and permeability of the metal ( $\rho_m, \sigma_m, \mu_m$ ) and polymer ( $\rho_p, \sigma_p, \mu_p$ ) are as shown. The total thickness of the laminated structure is  $T$ .

layers ( $i + 1$ ) is one more than that of the polymer layers ( $i$ ), as shown in Figure 3.

After deposition of all layers, the photoresist mold is removed, and the patterned multilayer laminated stacks can either be mechanically detached or left on the surface for electrical conductivity measurements.

### III. MATERIAL SELECTION AND DEPOSITION PARAMETERS

We first choose a proper set of metallic and interlayer material to illustrate the utility of the process. The materials set is chosen with a laminated magnetic core application in mind.

#### A. Metallic Material

A ferromagnetic metallic alloy, permalloy ( $\text{Ni}_{80}\text{Fe}_{20}$ ) [4], is chosen as the metallic material due to its high saturation flux density ( $\sim 1$  T), high relative permeability (typical  $\mu_r$  of 800-1000), low coercivity ( $< 2$  Oe), negligible magnetostriction, and well-known deposition chemistry.

#### B. Interlamination Insulation Material

Among many potential possibilities, anodically electropolymerized polypyrrole (PPy) was chosen as the interlamination insulation material due to (1) the ease of electrochemical deposition from aqueous electrolytes, (2) intermediate conductivity, and (3) the relatively dense, smooth nature of the deposits (compared to, e.g., fibrous polyaniline) [13]. In particular, poly(3,4-ethylenedioxythiophene) (PEDOT) derivatives that are useful in many applications due to their superior conductivities are not chosen in this application where only moderate conductivity is desired [14]. Cathodically deposited polypyrroles are not chosen since they are often porous [15]. Porous materials are undesirable as interlamination insulation materials since potential electrical shorts that may form between the neighboring magnetic layers during the lamination process could lead to a decrease of resistance between the magnetic layers.

#### C. Deposition Conditions

The deposition cycle in this process contains three steps, as shown in Figure 2: 1) cathodic electrodeposition of NiFe (on the underlying metal seed layer, or the previously deposited

polymer layer), 2) anodic polypyrrole electropolymerization, and 3) polymer surface activation by electrodeposition of a thin metallic layer, Ni, at a low deposition potential. Deposition is performed galvanostatically, while the electrochemical potential between the sample and the reference electrode is monitored. Both two-electrode (where the counter electrode acts as the reference) and three-electrode (with a standard Ag/AgCl reference electrode) approaches can be employed. In this work, non-sulfurized nickel sheets were used as counter electrodes for the metal electrodeposition, and platinum sputtered glass was used for the polymer deposition. The plating substrates are rinsed thoroughly with DI water between each step to avoid contamination of the next solution. The deposition area is defined by the patterned photoresist mold, which in turn defines the total plating current. The cathodic permalloy deposition is performed at a current density of 10 mA/cm<sup>2</sup>. The current density is chosen to achieve the desired Ni to Fe ratio (4:1), resulting in a plating efficiency of approximately 65% [16].

The deposition bath of PPy consists of an aqueous solution of pyrrole monomer and a supporting electrolyte, which is a pre-dissolved salt. Since the polymerization of pyrrole occurs anodically, the anion for the supporting electrolyte is often incorporated into the chains as deposition occurs. That anion can thus influence the mechanical and electrical properties of the resulting films. Saccharin (Sac), oxalate (Ox), salicylate (Sal), dodecylbenzenesulfonate (DBS), and chloride (Cl) based electrolytes have all been demonstrated as effective supporting anions in the literature [17]–[19]; however, salicylate was utilized in this study due reports of uniform film thicknesses with low surface roughness and potential for passivating the underlying metal layers during the anodic electropolymerization [20]–[22].

Polypyrrole deposition baths are prepared by first vacuum distilling pyrrole monomer to remove any oxidized contaminants, and then the adding the desired volume of distilled pyrrole into a freshly prepared electrolyte of sodium salicylate. The deposition of PPy is performed on the previously deposited NiFe layer during the sequential electrodeposition process. The bath composition and current density were chosen such that the polymer deposition uniformity (across the total patterned area) and the roughness of the deposited films are balanced. For example, a uniform PPy deposition is not achieved in the baths with insufficient pyrrole concentration (< 0.1M or 6.7 g/L pyrrole monomer), since the deposition reaction of PPy is overwhelmed by the oxidization of the underlying NiFe. On the contrary, the roughness of the PPy surfaces (which needs to be controlled to achieve well defined multilayer structures) tends to increase as a function of monomer concentration and current density. Thus, PPy deposition is completed at 2.5 mA/cm<sup>2</sup>.

The final step of a single deposition cycle is the cathodic surface activation. A low deposition potential Ni deposition process is designed to form a thin, uniform metallic layer on the polymer layer prior to the beginning of the next cycle (permalloy deposition). The Ni deposition bath contains a high concentration (1M) of NiCl<sub>2</sub> [17]. The deposition is performed at a low current density of 0.5 mA/cm<sup>2</sup>, and an elevated bath

TABLE I  
DEPOSITION BATH COMPOSITIONS FOR PERMALLOY ELECTRODEPOSITION, POLYMER ELECTROPOLYMERIZATION, AND SURFACE ACTIVATION VIA NICKEL STRIKE.  
ALL BATHS ARE AQUEOUS

Permalloy deposition bath		Polymer deposition bath		Surface activation bath (Ni strike bath)	
Material	Quantity [g/L]	Material	Quantity [g/L]	Material	Quantity [g/L]
NiSO <sub>4</sub> ·6H <sub>2</sub> O	200	Pyrrole	20	NiCl <sub>2</sub>	130
NiCl <sub>2</sub> ·6H <sub>2</sub> O	5			Boric acid	30
FeSO <sub>4</sub> ·7H <sub>2</sub> O	8	Sodium Salicylate	16	Saccharin	1
Boric acid	25				
Saccharin	3				
pH	~4	pH	~7	pH	~2.5

temperature (~45 °C) to achieve a uniform Ni film at a low deposition potential (~−0.7V vs. Ag/AgCl). The compositions of all deposition solutions are summarized in Table I.

#### IV. LAMINATION FABRICATION RESULTS

##### A. Multilayer Deposition Profiles

In order to determine the efficacy of the PPy – NiFe multilayer electroplating approach, the voltage profiles during deposition were measured, and the structures were characterized via optical and SEM microscopy. Figure 4 shows various deposition profiles for the materials being deposited in each part of the three-step electroplating process (per cycle).

For the permalloy, it is found that uniform NiFe deposition on the activated polymer surface is achieved at a potential comparable to the measured NiFe deposition potential on a metallic seed layer. A direct electrodeposition of permalloy on the previously deposited PPy layer has also been studied, using the identical deposition current profile. A relatively higher deposition voltage exceeding −1 V is observed. This leads to the inclusion of cations into the polymeric matrix and the exclusion (or de-doping) of the negative dopant anions that were trapped within the polymeric chain (the salicylate anions). Such a process can result in a further decrease of the polymer conductivity [20]. A sharp increase of the deposition potential up to −4 V is then observed, and the deposition quality is poor. Further, it was observed that during direct deposition of NiFe on PPy, the layers delaminated from the underlying substrate, likely due to the stress generated during the de-doping process. Thus, in order to obtain robust multilayer structures, passivation/activation of the PPy layer with an electrically conducting film is performed by means of the electrodeposition of a thin (~100-200 nm) Ni film at low potential before proceeding with NiFe plating.

##### B. Structural Characterization

Representative single layer films of each material as well as multilayer laminated structures were fabricated and characterized to determine material growth rates and layer

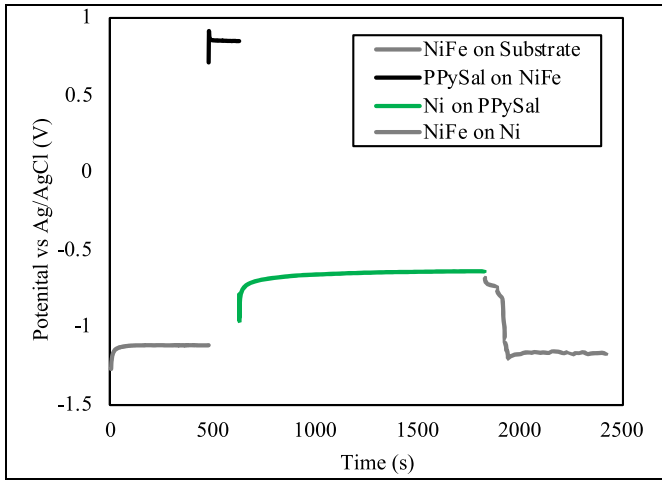


Fig. 4. Measured electrochemical potential for all layers against Ag/AgCl reference electrode.

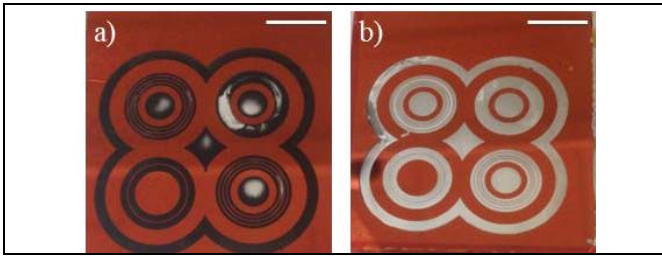


Fig. 5. Top-down optical images of a sample toroidal patterned area after a) NiFe on PPySal and b) NiFe on Ni on PPySal. The scale bar indicates 1 cm for both images.

uniformity within patterned molds and throughout the deposition processes. Top-down and cross-sectional SEM images were taken for structural characterization, and the deposition profiles were examined by SEM and profilometry, as shown in Figures 5 – 7. From the top down images in Figure 4 of actual samples after deposition, the beneficial effects of utilizing a Ni strike activation layer in the sequential deposition process can be observed.

The deposition was performed at batch-scale with the smallest feature sizes being a few tens of micrometers, corresponding to typical MEMS structures (Figure 6). The resulting films were uniform across the substrate area.

The thickness of each deposited layer was determined both during deposition of single layer films and as part of the multilayer fabrication process. The individual growth rates were characterized using profilometry of deposited films at constant plating current densities and deposition times. The deposition rate of NiFe ( $r_{\text{NiFe}}$ ) at  $10\text{mA}/\text{cm}^2$  within a mold was measured to be  $2.1\text{ nm/s}$ , which is consistent with observations in the literature [16]. The deposition rate of PPySAL at  $2.5\text{mA}/\text{cm}^2$  in the vertical direction ( $r_{\text{PPy},y}$ ) was measured to be  $7.5\text{ nm/s}$ . For comparison, a theoretical estimation of the deposition rate of polypyrrole is presented in Equation 2 [23]:

$$r_{\text{PPy},y} = \left( \frac{M_p + yM_{\text{dop}} - 2}{\delta(2 + y)F} \right) \cdot Jt \quad (2)$$

where  $M_p$  is the molecular weight of pyrrole,  $M_{\text{dop}}$  is the molecular weight of the dopant (the salicylate anion),  $y$  is the doping level (assumed to be 0.25 [24]),  $F$  is the Faraday

constant,  $\delta[\text{g}/\text{cm}^3]$  is the density of PPy (measured to be  $1.5\text{ g}/\text{cm}^3$ ),  $J[\text{mA}/\text{cm}^2]$  is the current density, and  $t[\text{s}]$  is the PPy deposition time. For a  $J$  of  $2.5\text{ mA}/\text{cm}^2$ , the calculated theoretical  $r_{\text{PPy},y}$  is  $7.65\text{ nm/s}$ , which is very close to the measured rate,  $7.5\text{ nm/s}$ .

While the growth rate, as measured in the center of the patterns, was consistent with the theoretical calculation (and was consistent both across patterns on a given substrate as well as across different substrates), it was observed (as seen in Figure 6d by the halo-like structure at the perimeter of the circular plating molds) that the thickness of deposited PPy layers at the edge of the mold was larger, indicating that lateral growth of PPy (where the lateral rate is represented by  $r_{\text{PPy},x}$ ) occurs during the electropolymerization process.

The measured  $r_{\text{PPy},x}$  is higher than  $r_{\text{PPy},y}$ , leading to a relatively large growth anisotropy,  $\alpha = r_{\text{PPy},x}/r_{\text{PPy},y}$ . This observation is in agreement with previous reports on the anisotropic electrochemical growth of conductive polymers [24]. As a result, the total achievable thickness of PPy within a mold (mold thickness,  $t_{\text{mold}}$ ) is limited to the summation of the total NiFe thickness ( $T_m$ ) and the total PPy thickness in the vicinity of the mold (i.e., the product of the growth anisotropy,  $\alpha$ , and the total thickness of the vertically grown PPy,  $T_p$ ), as described by Equation 3.

$$t_{\text{mold}} = \alpha T_p + T_m \quad (3)$$

An  $\alpha \approx 6$  is typically observed; therefore, a photoresist mold thicker than  $25\text{ }\mu\text{m}$  (the nominal maximum achievable mold thickness by a single spin coating of AZ4620) would be necessary to define a multilayer structure with  $T_p > 4\text{ }\mu\text{m}$  if any over-plating is not accepted.

The Ni strike layer growth rate was characterized at a current density of  $0.5\text{mA}/\text{cm}^2$  and measured to be  $0.15\text{ nm/s}$ . The slow growth rate is consistent with the low current density and potential necessary to protect and activate the PPy surface for subsequent layer deposition.

Supplementing the single layer growth rate studies, multilayer NiFe/PPy/Ni stacks were characterized using focused ion beam (FIB) generated cross-sections. For the purposes of these experiments, structures with 3 sets of NiFe/PPy/Ni multilayers with a finishing layer of NiFe were fabricated. Figure 7 shows a FIB cross-section of the sample structure (also shown in Figure 5). The individual layers of NiFe and PPy are clearly distinguished, and the thickness and thus deposition rate of both materials is relatively constant throughout the multilayer deposition process.

### C. Electrical Characterization

Electrical characterization of permalloy and/or PPySal was performed to assess the potential utility of these electrodeposited laminated structures and determine the degree of achieved anisotropy. A schematic of the experimental setup of each measurement type is shown in Figure 8.

1) *Lateral Conductivity*: The lateral conductivities of electrodeposited permalloy and PPy were measured at DC using a 4-point probe. The film-of-interest (either  $1\text{ }\mu\text{m}$ -thick NiFe or  $5\text{ }\mu\text{m}$ -thick PPy) was electrodeposited on a copper seed layer and then mechanically detached, after which

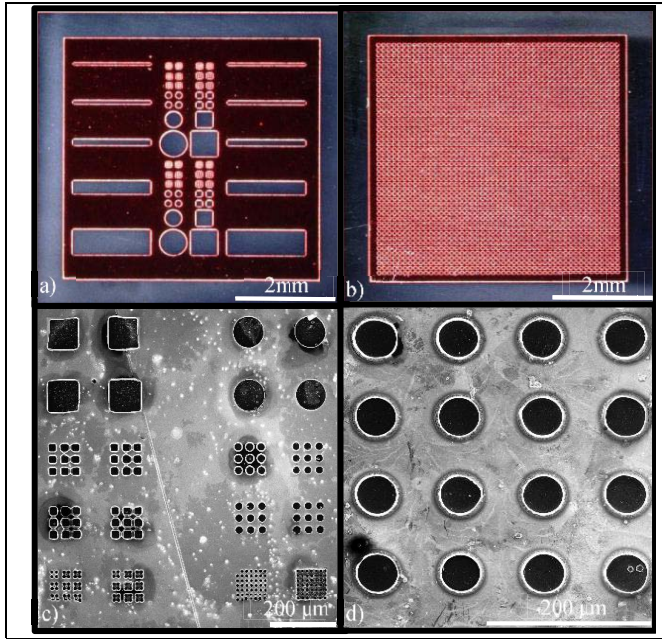


Fig. 6. An optical image of PPy-Sal electrodeposited through sample mold patterns of various geometries. a) A top-down optical image of a test photoresist mold with patterns of varied widths and arrays. b) An optical image of PPy-Sal electrodeposited through a large area of symmetric 50-micron circle patterns. c) SEM image of uniquely defined PPy growth with feature sizes from 10-50 microns. d) SEM image of PPy growth in 50  $\mu\text{m}$  circular patterns. Growth is uniform both across a single substrate as well as from substrate to substrate, but larger thicknesses at mold pattern edges are observed.

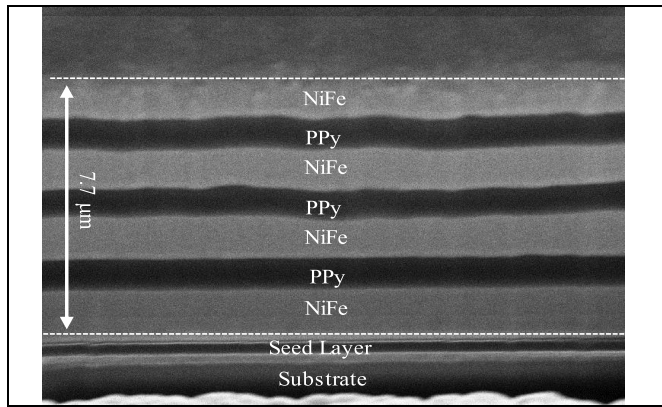


Fig. 7. SEM Cross-sectional image of 3 sets of laminations with an added top layer of NiFe.

the copper seed layer was selectively removed in a saturated  $\text{CuSO}_4/\text{NH}_4\text{OH}$ -based etchant. The etchant is prepared by adding 240 g  $\text{CuSO}_4$  to 1L of 30%  $\text{NH}_4\text{OH}$ , allowing the mixture to sit overnight, and then removing any precipitates.

The measured permalloy conductivity,  $\sigma_m$ , is  $1.1 \times 10^7 \text{ S/m}$  and the polymer conductivity,  $\sigma_{p,x}$ , is 437 S/m [25], [26]. Utilization of a 4-point probe eliminated the effect of probe contact resistance on the measurement; further, it was observed that the lateral conductivity was independent of the applied voltage.

The effective lateral conductivity of a laminated structure consisting of NiFe and PPy multilayer stacks ( $\sigma_x$ ) can be calculated based on the summation of the conductance of

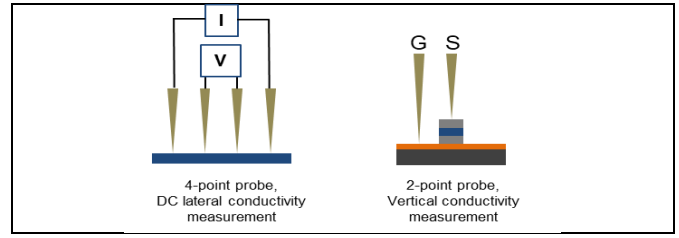


Fig. 8. Schematics of the electrical measurement configurations for DC lateral and DC/AC vertical conductivity.

PPy and NiFe layers ( $\sigma_{p,x}$  and  $\sigma_m$ , respectively), as shown in Equation 4.

$$\sigma_x = \sigma_m \gamma + \sigma_{p,x}(1-\gamma) \quad (4)$$

In Equation 4,  $\gamma$  is the fill factor, which is the fraction of the total core thickness that is comprised of the magnetic material. Given a fill factor of 0.5 (as shown in Figure 7), and since  $\sigma_m/\sigma_{p,x} = 2.5 \times 10^4 \gg 1$ , the conductivity of the polymer in the lateral direction can be neglected. This would be true even at high frequencies, where the conductivities of typical conductive polymers are enhanced [24]. Hence, we can assume Equation 5 holds true for arbitrary laminations of NiFe and PPySal.

$$\sigma_x \approx \sigma_m \gamma \quad (5)$$

2) *Vertical Conductivity*: The vertical conductivities ( $\sigma_y$ ) of the laminated structures were characterized both at DC and AC. In order to measure the vertical conductivities of the multilayer constructs, two types of patterns were created. The first consists of isolated, 50  $\mu\text{m}$  diameter cylinders comprising an electroplated stack of NiFe, PPy, and NiFe layers using the same plating conditions described above. For reference, Pt-metallized stacks of the same geometry were also fabricated. These stacks consist of sputtered Pt seed layer, electropolymerized PPy on the seed layer, and a top sputtered Pt electrode.

DC measurements were performed for both the NiFe/PPy and Pt/PPy stacks to compare the electrical behavior when the polymer is contacted by metals with different work functions. AC measurements were conducted for the NiFe/PPy stacks for analysis of the electrodeposited multilayers at high frequency. Before measuring each sample, the probe tips were calibrated on an un-patterned surface of permalloy to control for the contact resistances between the probes and the permalloy surfaces. The measured DC resistances and AC impedances are attributed to the PPy insulation layer, as those of the highly conductive NiFe are neglected.

Sample DC I-V curves of NiFe/PPy/NiFe and Pt/PPy/Pt stacks are presented in Figures 9a and 9b, respectively. The DC I-V curve of the NiFe/PPy/NiFe laminated structure (Figure 9a) is non-linear (but nearly symmetric with respect to 0 V), displaying polymer/metal Schottky-like behavior with a turn-on voltage of approximately 0.5V. It is well known that conductive polymers may form a Schottky contact with metals possessing a relatively low work function [27]. In contrast,

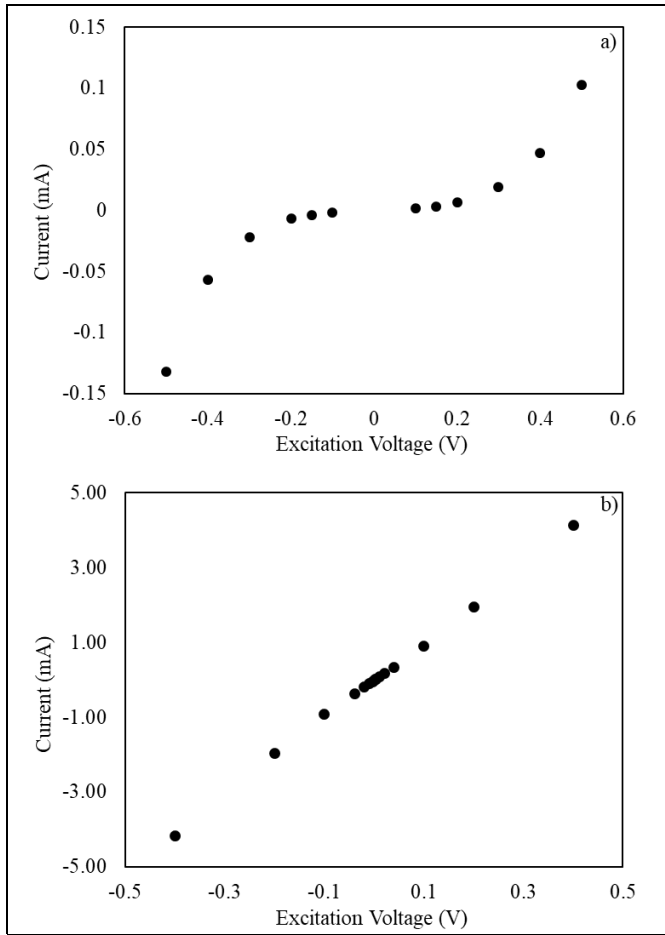


Fig. 9. (a) DC resistance characterization of a sample NiFe/PPy/NiFe stack, where each layer is  $1\mu\text{m}$  thick. The current through the stack increases exponentially in each direction. (b) DC resistance characterization of Pt/PPy/Pt stacks, where the PPy layer is  $1\mu\text{m}$  thick and the Pt layers are  $50\text{nm}$  thick. The current through the stack increases linearly.

the I-V curve of the corresponding Pt/PPy/Pt structure demonstrated ohmic behavior (Fig. 9b), consistent with the relatively high work function of Pt.

At low voltages, the conductivity of the NiFe/PPy/NiFe laminated structure at DC is approximately  $0.01\text{ S/m}$ , and the conductivity of the Pt/PPy/Pt multilayer stack at DC is  $4.4\text{ S/m}$ . The difference between the DC vertical conductivities of the two multilayer stacks is almost a factor of 500, indicating that the contact between the polymer and metal in a laminated multilayer material is crucial to determining its electrical performance.

The AC measurements were made by applying a sinusoidal excitation as a function of frequency and measuring the impedance magnitude and phase angle across stacked layers. This data is subsequently used to calculate the real and imaginary parts of the impedance. Sample impedance curves are shown in Figure 10.

As shown in Figure 10a and 10b, the measured impedance magnitude is relatively constant with a phase angle near zero at low frequencies and becomes small with phase angle approaching  $-90$  degrees at high frequencies. Such characteristics are compatible with a parallel resistance-capacitance model, as are the real and imaginary parts of the impedance

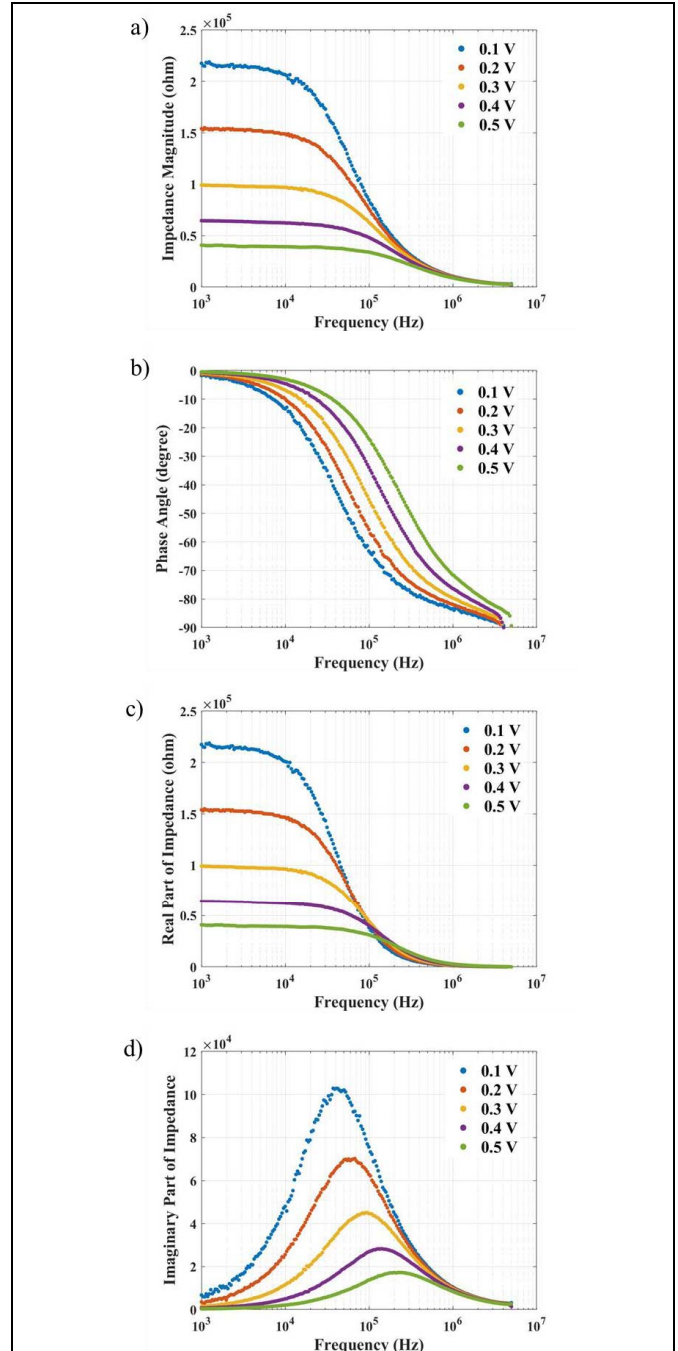


Fig. 10. (a) Impedance magnitude, (b) phase angle, (c) real part of impedance, and (d) imaginary part of impedance of cylindrical NiFe/PPy/NiFe stacks where the PPy layer is  $1.6\mu\text{m}$  thick.

shown in Figure 10c and 10d. The non-linear, non-ohmic behavior found in the low frequency regime of the AC impedance magnitude is in alignment with the polymer/metal Schottky-like behavior observed in DC characterization.

The effective magnitude  $\sigma_{p,y}$  of polymer AC conductivity in a multilayer composite can be defined using Equation 6:

$$|\sigma_{p,y}| = \frac{1}{\rho} = \frac{t}{(|Z|) \times (A)} \quad (6)$$

where  $A$  is the projected area of the laminated structure ( $\sim 2000\mu\text{m}^2$ ),  $t$  is the thickness of the PPy layer, and  $|Z|$  is the

magnitude of the measured impedance in the vertical direction of a single metal-PPy-metal multilayer stack. Because of both capacitive effects as well as the Schottky-like behavior of PPy with certain metals,  $\sigma_{p,y}$  could depend on contact metallurgy, frequency, and excitation level.

The calculated  $\sigma_{p,y}$  in a NiFe multilayer structure at low frequency ( $< 1$  kHz) ranges from 0.004 S/m (at 0.1 V excitation) to 0.02 S/m (at 0.5 V excitation) while at high frequency (1 MHz), it ranges from 0.08 S/m (at 0.1 V excitation) to 0.09 S/m (at 0.5 V excitation). For Pt contacts, the multilayer conductivity at low frequency is 4.4 S/m (Figure 8b). Even the highest values of PPy conductivity at high frequency and excitation yield significant conductivity anisotropy, exceeding  $10^6$  across the measured frequency range using an all-additive fabrication process.

## V. CONCLUSION

Metal/polymer laminated structures with designed microscale geometries were additively fabricated on various substrates in batch scale using sequential electrodeposition through photoresist molds. Desired anisotropic electrical material properties were achieved; in particular, the requirement of lateral to vertical conductivity anisotropy of  $10^6$  is achievable at frequencies of interest. The unique properties of the polypyrrole conductive polymer doped with salicylate anions enabled both sequential electrodeposition of metal and polymer layers and highly anisotropic vertical and lateral conductivities of the resulting multilayer structures, likely resulting from Schottky-like behavior of polypyrrole contacts with low work function metals or alloys. These characteristics show great promise for use of these laminated stacks in microfabricated inductor cores that operate at high frequencies, thus contributing to the reduction of inductor volumes needed in typical converters needed to integrate MEMS power sources and sensing or actuation systems.

## REFERENCES

- [1] M.-J. Pan and C. A. Randall, "A brief introduction to ceramic capacitors," *IEEE Elect. Insul. Mag.*, vol. 26, no. 3, pp. 44–50, May 2010.
- [2] X. Yu *et al.*, "Watt-level wireless power transfer based on stacked flex circuit technology," in *Proc. IEEE 61st Electron. Compon. Technol. Conf. (ECTC)*, May 2011, pp. 2185–2191.
- [3] M. Kim, J. Kim, F. Herrault, R. Schafer, and M. G. Allen, "A MEMS lamination technology based on sequential multilayer electrodeposition," *J. Micromech. Microeng.*, vol. 23, no. 9, Sep. 2013, Art. no. 095011.
- [4] J. Kim *et al.*, "Nanolaminated permalloy core for high-flux, high-frequency ultracompact power conversion," *IEEE Trans. Power Electron.*, vol. 28, no. 9, pp. 4376–4383, Sep. 2013.
- [5] S. Shin, J.-H. Kim, J. Jeong, T. M. Gwon, S.-H. Lee, and S. J. Kim, "Novel four-sided neural probe fabricated by a thermal lamination process of polymer films," *J. Neurosci. Methods*, vol. 278, pp. 25–35, Feb. 2017.
- [6] M. Kim, J. Kim, and M. G. Allen, "Composite materials with controllable macromechanical properties based on MEMS-assisted structural manipulation of low-dimensional subcomponents," in *Proc. IEEE 30th Int. Conf. Micro Electro Mech. Syst. (MEMS)*, Jan. 2017, pp. 708–711.
- [7] D. Yao, C. G. Levey, R. Tian, and C. R. Sullivan, "Microfabricated V-groove power inductors using multilayer Co–Zr–O thin films for very-high-frequency DC–DC converters," *IEEE Trans. Power Electron.*, vol. 28, no. 9, pp. 4384–4394, Sep. 2013.
- [8] J.-W. Park, F. Cros, and M. G. Allen, "A sacrificial layer approach to highly laminated magnetic cores," in *Tech. Dig. MEMS IEEE Int. Conf., 15th IEEE Int. Conf. Micro Electro Mech. Syst.*, Jan. 2002, pp. 380–383.
- [9] R. Anthony, C. O' Mathúna, and J. F. Rohan, "MEMS based electrochemical process for fabrication of laminated micro-inductors on silicon," *Microelectron. Eng.*, vol. 155, pp. 33–38, Apr. 2016.
- [10] M. Brunet, T. O'Donnell, A. M. Connell, P. McCloskey, and S. C. O. Mathuna, "Electrochemical process for the lamination of magnetic cores in thin-film magnetic components," *J. Microelectromech. Syst.*, vol. 15, no. 1, pp. 94–100, Feb. 2006.
- [11] M. Kim and M. G. Allen, "Interlamination insulation design considerations for laminated magnetics operating at high frequencies," *IEEE Trans. Magn.*, vol. 55, no. 8, pp. 1–11, Aug. 2019.
- [12] J.-M. Quemper *et al.*, "Permalloy electroplating through photoresist molds," *Sens. Actuators A, Phys.*, vol. 74, nos. 1–3, pp. 1–4, Apr. 1999.
- [13] V. Gupta and N. Miura, "High performance electrochemical supercapacitor from electrochemically synthesized nanostructured polyaniline," *Mater. Lett.*, vol. 60, no. 12, pp. 1466–1469, Jun. 2006.
- [14] X. Crispin *et al.*, "The origin of the high conductivity of poly(3,4-ethylenedioxythiophene)–poly(styrenesulfonate) (PEDOT–PSS) plastic electrodes," *Chem. Mater.*, vol. 18, no. 18, pp. 4354–4360, Sep. 2006.
- [15] D. H. Nam, M. J. Kim, S. J. Lim, I. S. Song, and H. S. Kwon, "Single-step synthesis of polypyrrole nanowires by cathodic electropolymerization," *J. Mater. Chem. A*, vol. 1, no. 27, pp. 8061–8068, 2013.
- [16] K. Y. Kok, C. M. Hangarter, B. Goldsmith, I. K. Ng, N. B. Saidin, and N. V. Myung, "Synthesis and characterization of electrodeposited permalloy (Ni80Fe20)/Cu multilayered nanowires," *J. Magn. Magn. Mater.*, vol. 322, no. 24, pp. 3876–3881, Dec. 2010.
- [17] T. Miyake, M. Kume, K. Yamaguchi, D. P. Amalnerkar, and H. Minoura, "Electrodeposition of Cu/Ni–P multilayers by a single bath technique," *Thin Solid Films*, vol. 397, nos. 1–2, pp. 83–89, Oct. 2001.
- [18] E. W. H. Jager, "Microfabricating conjugated polymer actuators," *Science*, vol. 290, no. 5496, pp. 1540–1545, Nov. 2000.
- [19] H.-S. Min *et al.*, "Fabrication and properties of a carbon/polypyrrole three-dimensional microbattery," *J. Power Sources*, vol. 178, no. 2, pp. 795–800, Apr. 2008.
- [20] J. Petitjean, S. Aeiyaich, J. C. Lacroix, and P. C. Lacaze, "Ultra-fast electropolymerization of pyrrole in aqueous media on oxidizable metals in a one-step process," *J. Electroanal. Chem.*, vol. 478, nos. 1–2, pp. 92–100, Dec. 1999.
- [21] A. Srinivasan, P. Ranjani, and N. Rajendran, "Electrochemical polymerization of pyrrole over AZ31 mg alloy for biomedical applications," *Electrochimica Acta*, vol. 88, pp. 310–321, Jan. 2013.
- [22] E. Hermelin, J. Petitjean, S. Aeiyaich, J. C. Lacroix, and P. C. Lacaze, "Industrial polypyrrole electrodeposition on zinc-electroplated steel," *J. Appl. Electrochem.*, vol. 31, no. 8, pp. 905–911, 2001.
- [23] L. M. M. dos Santos, J. C. Lacroix, K. I. Chane-Ching, A. Adenier, L. M. Abrantes, and P. C. Lacaze, "Electrochemical synthesis of polypyrrole films on copper electrodes in acidic and neutral aqueous media," *J. Electroanal. Chem.*, vol. 587, no. 1, pp. 67–78, Feb. 2006.
- [24] G. Sabouraud, S. Sadki, and N. Brodie, "The mechanisms of pyrrole electropolymerization," *Chem. Soc. Rev.*, vol. 29, no. 5, pp. 283–293, 2000.
- [25] S. Demoustier-Champagne and P.-Y. Stavaux, "Effect of electrolyte concentration and nature on the morphology and the electrical properties of electropolymerized polypyrrole nanotubules," *Chem. Mater.*, vol. 11, no. 3, pp. 829–834, Mar. 1999.
- [26] D. M. C. Nicholson *et al.*, "Magnetic structure and electronic transport in permalloy," *J. Appl. Phys.*, vol. 81, no. 8, pp. 4023–4025, Apr. 1997.
- [27] J. Lei, W. Liang, C. J. Brumlik, and C. R. Martin, "A new interfacial polymerization method for forming metal/conductive polymer Schottky barriers," *Synth. Met.*, vol. 47, no. 3, pp. 351–359, Jun. 1992.